JAASCI
http://jaasci.com
JOURNAL OF ADVANCED APPLIED SCIENCES
e-ISSN: 2979-9759
PRENSİP
https://prensip.gen.tr

RESEARCH ARTICLE

Decoupling Intergranular Weak-Links and Intragranular Flux Pinning in Bulk Bi-2212 Superconductors: A Two-Component Exponential Model Approach

Mehmet Ali Aksan[1]✉ • Gokhan Kirat[2]

[1]İnönü University, Faculty of Arts and Sciences, Department of Physics, Malatya/Türkiye
[2]İnonü University, Scientific and Technological Research Center, Malatya/Türkiye

ARTICLE INFO

Article History
Received: 28.05.2026
Accepted: 15.06.2026
First Published: 28.06.2026

Keywords
Bi-2212 superconductors
Critical current density
Flux pinning
Intergranular - intragranular J_c
Two-component exponential model

ABSTRACT

In this study, the influence of sintering time on the structural, microstructural and magneto-transport properties of bulk $Bi_2Sr_2CaCu_2O_{8+\delta}$ (Bi-2212) HT_c superconductors synthesized by the solid-state reaction method was investigated using Two-Component Exponential Model. The samples prepared were heat treated at 840 ºC for two different sintering durations: 60 h (S60) and 120 h (S120). XRD analyses showed that both samples have tetragonal symmetry and increasing the sintering duration to 120 h markedly reduced secondary impurity phases, such as $BiSr_3O_{5.4}$ and $Bi_2Ca_2O_5$, thereby enhancing phase purity and crystallographic order. Furthermore, thermally activated oxygen desorption during prolonged heat treatment caused an expansion of the *c*-axis lattice parameter (from 30.62 Å to 30.68 Å), indicating a transition from the overdoped regime to the optimally doped region. The average crystallite size, estimated using the Scherrer method, increased from 38 nm to 45 nm, while Williamson–Hall analysis revealed a significant reduction in internal strain and defect density. SEM micrographs demonstrated the formation of characteristic platelet-like grain morphology and improved grain interlocking resulting from anisotropic grain growth. Analysis of the transport mechanism based on a semi empirical Two-Component Exponential Model showed that the 120 h sintering protocol not only enhanced the Josephson current transport capability (J_c^{wl}) at the macroscopic level through grain-boundary purification, but also improved the stability of flux pinning centers (H_{int}) at the microscopic level by optimizing nanoscale intragrain defects and oxygen stoichiometry, thereby yielding a dual improvement in high-field magnetic performance.

Please cite this paper as follows:

Aksan, M. A., & Kirat, G. (2026). Decoupling intergranular weak-links and intragranular flux pinning in bulk Bi-2212 superconductors: A two-component exponential model approach. *Journal of Advanced Applied Sciences*, *5*(1), 24-33. https://doi.org/10.61326/jaasci.v5i1.495

1. Introduction

The discovery of high-temperature (HT_c) superconductivity in 1986 became a milestone in scientific world. Subsequently, the discovery of superconductivity in the rare-earth-free Bi–Sr–Ca–Cu–O (BSCCO) system attracted considerable interest (Maeda et al., 1988). Among the various phases of the BSCCO system, $Bi_2Sr_2CaCu_2O_{8+\delta}$ (Bi-2212) system has emerged as one of the most technologically important cuprate superconductors. Although its critical transition temperature ($T_c \approx 80$ K) is lower than that of several other cuprate systems, its superior thermodynamic phase stability, relatively broad synthesis window, ease of processing into bulk, wire and ribbon forms, and remarkable performance under high external magnetic fields have made it a key material for both fundamental quantum-mechanical studies and industrial high-field magnet applications.

✉ Correspondence
E-mail address: mehmet.aksan@inonu.edu.tr

The applicability of bulk polycrystalline Bi-2212 superconductors in high-current engineering applications is critically constrained by the granular nature of the material, weak mechanical properties and pronounced crystallographic anisotropy. In such polycrystalline systems, grain boundaries formed between randomly oriented adjacent grains, along with amorphous secondary phases preferentially segregated at these interfaces during synthesis, markedly degrade the superconducting transport characteristics (Hilgenkamp & Mannhart, 2002). Such grain boundaries act as Josephson weak-link barriers that hinder the continuous circulation of macroscopic supercurrent and limit quantum-mechanical tunneling between adjacent grains. Under an external magnetic field, superconducting phase coherence across the weak-link structures rapidly deteriorates, resulting in a pronounced suppression of the critical current density (J_c) even at low magnetic fields (Peterson & Ekin, 1988). In this regard, precise control of heat-treatment (sintering) parameters to optimize solid-state diffusion kinetics and grain-boundary migration (Ostwald ripening) plays a crucial role in promoting morphological grain interlocking, enhancing crystallographic texturing and narrowing the effective thickness of Josephson weak-link barriers.

Beyond the structural and microstructural morphology, the interstitial oxygen content within the Bi-2212 crystal lattice plays a critical role in determining the electronic properties of the system. Bi-2212 systems prepared by conventional routes in an ambient air atmosphere inherently tend to stay in an overdoped regime, where the hole concentration in the CuO_2 planes deviates from its optimal level, leading to a suppression of Cooper pair density and consequently a reduction in the superconducting transition temperature (T_c) (Ross, 2005). Extended sintering duration facilitates controlled oxygen desorption from the crystal lattice via thermally activated processes. The accompanying expansion of the *c*-axis shifts the system from the overdoped regime to the optimally doped state, consequently improving both the intrinsic (intra-grain) superconducting characteristics of the material and the macroscopic Meissner shielding fraction.

The layered crystal structure of Bi-2212 gives rise to highly complex magnetic vortex (flux-line) dynamics. Due to the large anisotropy parameter, independent two-dimensional (2D) pancake vortex structures confined within individual CuO_2 planes dominate instead of continuous three-dimensional (3D) flux lines throughout the material (Clem, 1991). At high-temperatures and high-magnetic-fields, these 2D pancake vortices readily decouple due to thermal fluctuations and Lorentz-force-driven dynamics, resulting in significant flux creep and consequently strong energy dissipation within the superconducting matrix (Blatter et al., 1994). Maintaining the current-carrying capability of the system requires a transition of the vortex matter from a weakly pinned, ordered Bragg glass phase into a disordered but collectively pinned vortex glass phase with strong flux-pinning centers (Fisher et al., 1991). This transition and stability are directly governed by the optimization of homogeneously distributed nanoscale point defects and oxygen vacancies within the crystal lattice.

In the literature, numerous studies have qualitatively investigated the influence of sintering time on the structural properties of Bi-2212 superconductors (Yang et al., 2016; Zhang et al., 2010), however, the quantitative decoupling of macroscopic weak-link transport and microscopic flux-pinning dynamics in relation to time-dependent thermal processing kinetics remains limited (Kametani et al., 2011; Wang et al., 2018). To elucidate this complex transport mechanism, the experimental magnetic-field dependence of the critical current density ($J_c - H$) can be analyzed with a semi-empirical double-exponential model that simultaneously accounts for intergranular (weak-link) and intragranular contributions. This model enables the quantitative decoupling of the Josephson coherence field (H_{wl}), which characterizes the magnetic-field sensitivity of weak links and the intragranular flux-pinning parameter (H_{int}), which represents the high-field pinning strength within grains.

In this study, bulk Bi-2212 superconducting samples were sintered at a constant temperature of 840 °C for two different durations, 60 h (S60) and 120 h (S120). The primary objective of the work is not only to investigate the effects of extended solid-state diffusion time on crystallographic lattice parameters, microstructural grain-boundary evolution and magnetic shielding capability, but also to quantitatively elucidate the corresponding variations in the model parameters H_{wl} and H_{int}. In this way, the multi-scale impact of sintering time on quantum mechanical phase locking and vortex glass stability is presented within an integrated modeling framework, providing a new physical perspective for predicting the high-field performance limits of bulk cuprate superconductors.

2. Experimental

In this work, the $Bi_2Sr_2CaCu_2O_{8+\delta}$ (Bi-2212) superconducting system was prepared by the conventional solid-state reaction route using high-purity Bi_2O_3, $SrCO_3$, $CaCO_3$ and CuO precursor powders (99.99%). After weighing according to the desired stoichiometric ratios and thorough mixing in an agate mortar, the powders were subjected to calcination at 800 °C for 24 h. The calcined powders were then finely ground, followed by a second calcination treatment at 820 °C for 24 h. The calcined powders were pelletized into circular disk-shaped pellets. Finally, the samples were placed inside a quartz tube and the pellets were subsequently sintered at a constant temperature of 840 °C for two different durations, 60 h and 120 h, to investigate the influence of thermal processing time on structural, magnetic and critical current density properties. It should be emphasized that a pressure of 10 tons was applied during the pelleting process.

The crystallographic structure of the sintered samples was analyzed by X-ray diffraction (XRD) using a Rigaku Miniflex 600 diffractometer equipped with Cu-K_α radiation (λ = 1.5406 Å). The surface morphology, anisotropic grain formations and microstructural characteristics were investigated using a Leo-Evo 40 scanning electron microscope (SEM). Superconducting properties were evaluated by temperature-dependent magnetization (M–T) under a constant external magnetic field of 50 Oe following the Zero-Field-Cooled (ZFC) protocol and magnetic-field-dependent magnetization (M–H) measurements performed with a vibrating sample magnetometer (VSM) integrated into a 9 T Quantum Design Physical Property Measurement System (PPMS).

The magnetic-field dependence of the critical current density ($J_c - H$), obtained from the magnetic hysteresis loops, was analyzed with a semi-empirical Two-Component Exponential Model to elucidate the complex transport behavior of the superconducting matrix. The applied modeling approach made it possible to quantitatively decouple the multi-scale effects of prolonged heat treatment on macroscopic weak-link transport and microscopic flux-pinning dynamics.

3. Results and Discussion

Figure 1 shows the XRD patterns of $Bi_2Sr_2CaCu_2O_{8+\delta}$ (Bi-2212) superconducting samples sintered at 840 ºC for 60 h (S60) and 120 h (S120). Diffraction peak indexing was performed using the standard JCPDS card for the Bi-2212 phase (No. 80-0396), confirming that all major reflections correspond to a tetragonal crystal structure in agreement with previous studies (Maeda et al., 1988; Tarascon et al., 1988). Bi-2212 crystallizes in a body-centered tetragonal sub-cell with the space group I4/mmm (No. 139) (Liang et al., 1988).

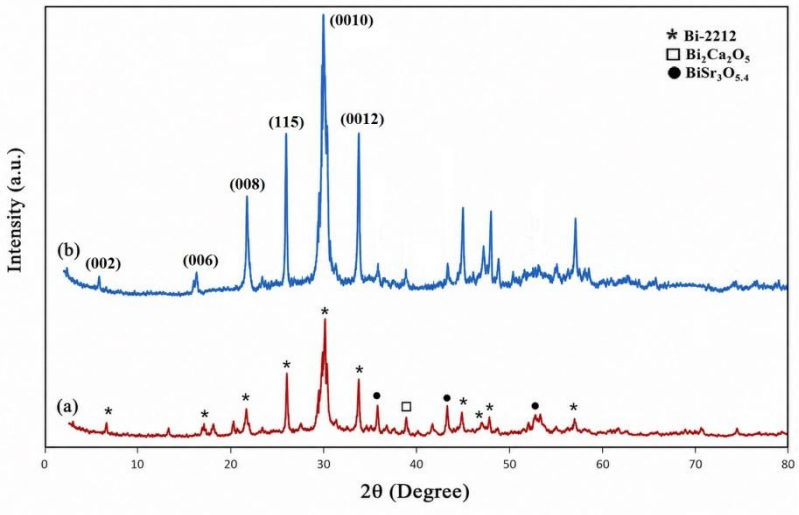

Figure 1. XRD patterns of Bi-2212 samples sintered at 840 ºC for (a) 60 h (S60) and (b) 120 h (S120).

Using the least-squares refinement method, the unit cell parameters of the S60 sample were calculated to be $a = b \approx$ 3.814 Å and $c \approx$ 30.62 Å ($c/a \approx$ 8.03), consistent with the ideal tetragonal unit-cell structure of Bi-2212 (Tarascon et al., 1988). For the S120 sample, the lattice parameters were determined to be $a = b \approx$ 3.816 Å and $c \approx$ 30.68 Å ($c/a \approx$ 8.04). The slight expansion of the *c*-axis obtained in S120 sample is attributed to thermally induced oxygen desorption during prolonged heat treatment. A decrease in the interstitial oxygen concentration in the Bi–O layers weakens the interlayer electrostatic interactions, thereby leading to *c*-axis expansion and shifting the system from the overdoped regime to the optimally doped superconducting regime (Argyriou et al., 1996; Ross, 2005). The optimization of oxygen stoichiometry shifts the hole concentration in the CuO_2 planes toward its optimal level in the superconducting phase diagram, thereby increasing both the density of states at the Fermi level and the Cooper pair density. This electronically stabilized lattice state is the main reason for the enhancements in superconducting transition temperature (T_c) and critical current density (J_c), which will be discussed in later sections. The unit-cell volumes were found to be approximately 445.42 Å³ for the S60 sample and 446.76 Å³ for the S120 sample. These results obviously show that prolonged sintering does not lead to any significant structural degradation or lattice distortion.

The strongest reflections indexed to the (0 0 2), (0 0 6), (0 0 8), (0 0 10), (0 0 12) and (1 1 5) planes are characteristic signatures of the layered perovskite structure of Bi-2212. Compared with the S60 sample, the S120 sample exhibits noticeably increased peak intensities, reflecting improved phase purity and a higher degree of crystallographic ordering achieved due to prolonged sintering. This behavior is consistent with the kinetic framework in which prolonged sintering promotes solid-state diffusion and reaction kinetics, resulting in the gradual reduction of residual intermediate and secondary

phases and consequently enhancing the crystallographic ordering of the system (Heeb et al., 1993).

In the S60 sample, the diffraction peaks attributed to secondary impurity phases such as $BiSr_3O_{5.4}$ and $Bi_2Ca_2O_5$ were obtained, arising from incomplete reactions. However, in the S120 sample, the volume fraction of these secondary phases is significantly suppressed. This suggests that Bi-2212 phase formation at 840 ºC is governed by slow reaction kinetics and that a prolonged sintering protocol of 120 h is essential to drive the system toward a thermodynamically more stable, nearly single-phase Bi-2212 state.

The average crystallite size (D) was calculated using the Scherrer equation (Scherrer, 1918):

$$D = K\lambda/\beta_{hkl}Cos\theta \quad (1)$$

where K is a dimensionless shape factor, with a value close to unity in general, λ is the wavelength of the incident X-ray radiation (1.5406 Å), β_{hkl} is the line broadening at half the maximum intensity (FWHM) and θ is the Bragg angle. Considering the anisotropic crystal structure, the (0 0 10) reflection was selected to estimate the crystallite size along the *c*-axis (i.e., perpendicular to the CuO_2 planes). The resulting values were D ≈ 38 nm for the S60 sample and D ≈ 45 nm for the S120 sample. The increase in crystallite size confirms grain growth during prolonged sintering, which enhances intergranular connectivity. To systematically distinguish the individual contributions of crystallite size and lattice microstrain to the diffraction peak broadening, Williamson–Hall (W-H) analysis was implemented according to the uniform deformation model (UDM) framework. The mathematical formulation is expressed as:

$$\beta_{hkl}Cos\theta = \frac{K\lambda}{D} + 4\varepsilon Sin\theta \quad (2)$$

where ε is the lattice microstrain. The calculated microstrain (ε) values obtained from Williamson–Hall analysis decrease from $\varepsilon \approx 2.1 \times 10^{-3}$ for S60 to $\varepsilon \approx 1.6 \times 10^{-3}$ for S120. This substantial reduction directly reflects the relaxation of internal stresses and lattice defects generated during the solid-state synthesis, confirming a significant enhancement in the long-range crystallographic order and overall crystallinity with prolonged sintering time.

The surface morphology and microstructural characteristics of both Bi-2212 samples were examined using the SEM micrographs presented in Figure 2. The images clearly reveal characteristic platelet-like grain morphology, which is a well-known feature of Bi-based cuprate superconductors. This morphology originates from the highly anisotropic crystal structure of the Bi-2212 phase, in which strong covalent bonding within the CuO_2 planes promotes preferential and faster growth along the *ab*-plane.

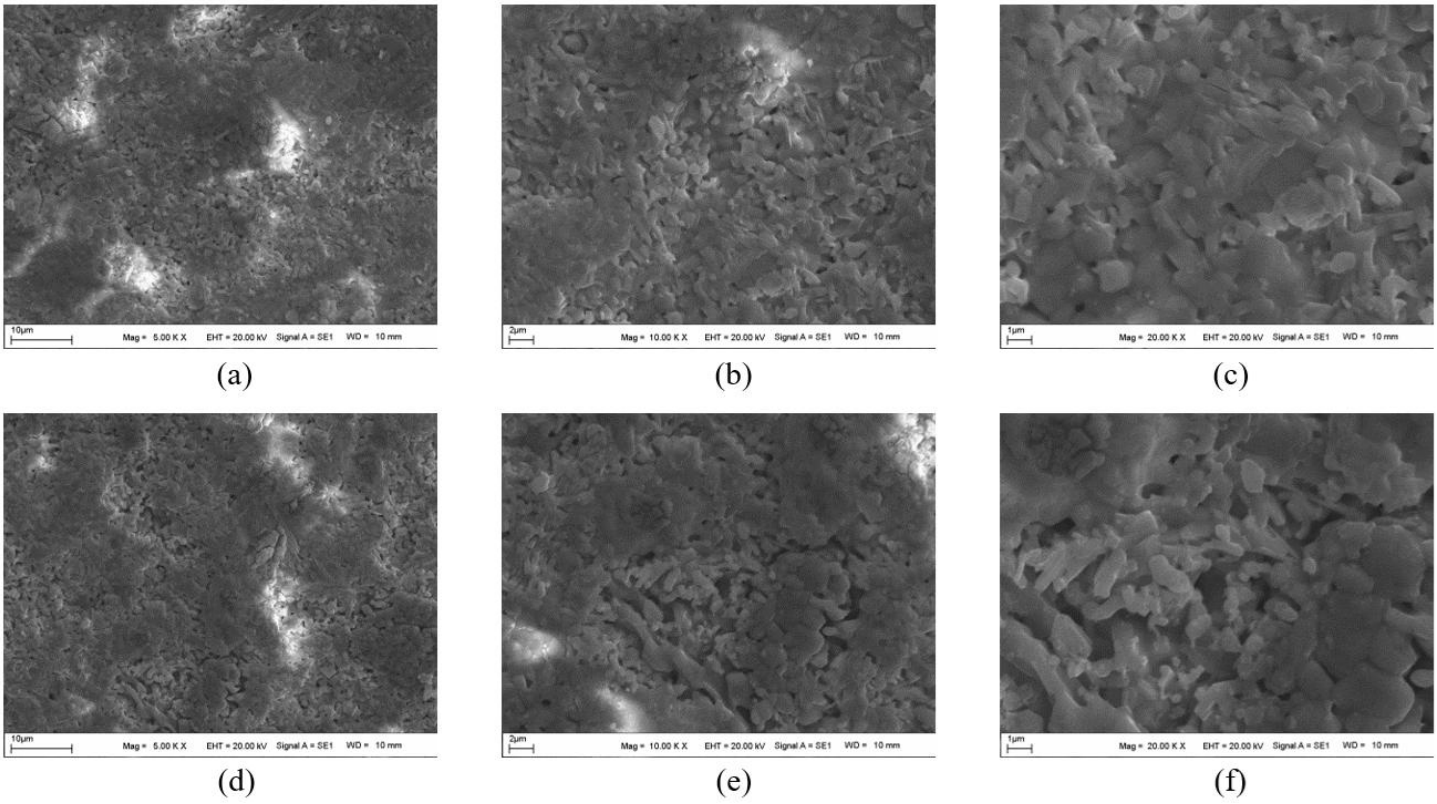

Figure 2. SEM micrographs of Bi-2212 samples sintered at 840 ºC for 60 h (a–c) and 120 h (d–f), recorded at magnifications of 5000×, 10000× and 20000×, respectively.

The SEM micrographs of the S60 sample (Figure 2a–c) show a microstructure consisting of thin platelet-like grains with lateral dimensions in the range of approximately 0.5–2 μm. The grains exhibit a highly random orientation, while uniformly distributed micro-porosities are observed on the sample surface. Although sintering of 60 h is sufficient for the formation of the Bi-2212 phase, mass transport, densification and grain growth processes remain incomplete. Moreover, the irregular nanoscale inclusions which are generally observed at grain boundaries are associated with secondary impurity phases such as $BiSr_3O_{5.4}$ and $Bi_2Ca_2O_5$, detected in the XRD analyses (Garnier et al., 1999).

In the S120 sample sintered for 120 h, a pronounced microstructural evolution is observed (Figure 2d–f). The grains grow along the *ab*-plane, reaching lateral dimensions of approximately 1–4 μm. This morphological improvement directly confirms the increase in crystallite size along the *c*-axis calculated using the Scherrer equation. The prolonged sintering promotes solid-state diffusion kinetics and grain-boundary migration, leading to enhanced intergranular interlocking and the formation of a larger effective contact area, thereby reducing weak-link effects in superconducting transport (Garnier et al., 1999). The improved crystallographic texturing and the reduction of secondary phases effectively decrease the thickness of the Josephson tunneling barrier. This microstructural improvement hinders the rapid decrease of the critical current density, J_c , at low magnetic fields and constitutes a key factor responsible for the increase in the intergranular weak-link characteristic field (H_{wl}), as given in the model parameters.

On the other hand, prolonged sintering leads to the coalescence of small pores into larger, localized macropores (Figure 2f). Despite the presence of such macropores in the S120 sample, the significantly enhanced diamagnetic signal observed in the M–T measurements indicates a higher shielding volume, which can be attributed to the increased grain size, stronger intergranular mechanical interlocking and higher phase purity. The localization of pores within the microstructure, without interrupting continuous current percolation paths, together with the improved grain quality, ultimately leads to an overall improvement in superconducting performance.

The temperature-dependent DC magnetization (M–T) results are showed in Figure 3. Both samples exhibit a pronounced diamagnetic transition characteristic of superconductivity; however, notable differences are observed between the S60 and S120 samples with respect to the superconducting transition temperature (T_c) and the Meissner shielding fraction.

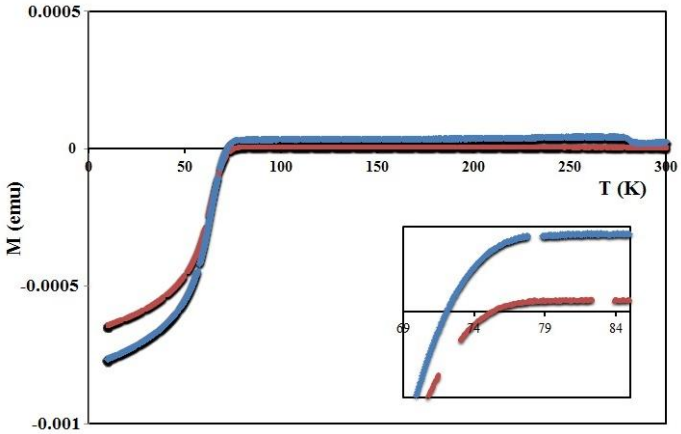

Figure 3. Temperature-dependent magnetization (M–T) curves of the samples sintered at 840 ºC for (a) 60 h (red curve) and (b) 120 h (blue curve).

As shown in the inset of Figure 3, which shows the reduced temperature range between 69 and 84 K, the onset superconducting transition temperature ($T_{c,onset}$) for the S60 sample (red curve) is found to be ~75 K. This value is below the maximum T_c value (~85 K) reported for optimally doped Bi-2212 compounds. For the S120 sample (blue curve), however, $T_{c,onset}$ increases to approximately 80 K upon prolonging the sintering duration to 120 h.

The observed increase in T_c is directly associated with the lattice parameter variations obtained from the XRD analysis. Bi-2212 system synthesized in ambient air typically exhibits an overdoped oxygen state, which suppresses the T_c temperature. Prolonged heat treatment of 120 h facilitates controlled oxygen desorption from the crystal lattice, consistent with the *c*-axis expansion observed in the XRD results. As a consequence, the system shifts from the overdoped regime toward the optimally doped regime, leading to an increase in the $T_{c,onset}$ value (Ross, 2005). Moreover, the sharper and steeper diamagnetic transition exhibited by the S120 sample, characterized by a narrower transition width (ΔT_c), indicates a closer convergence between the intrinsic intra-grain superconducting transition

temperature and the intergranular Josephson phase-locking temperature, suggesting the formation of a more homogeneous superconducting matrix. This result provides strong experimental evidence that grain-boundary purification enhances macroscopic quantum coherence and allows it to remain robust against external magnetic fields even at elevated temperatures.

In addition, the low-temperature diamagnetic response of the S120 sample is larger than that of the S60 sample. This behavior provides clear evidence of a significant increase in the effective superconducting volume fraction (shielding fraction) in the S120 sample. The pronounced difference in diamagnetic response between the S60 and S120 samples is fully consistent with the microstructural evolution observed in the SEM analysis. In granular superconductors, the magnitude of the ZFC signal strongly depends on the quality of intergranular connectivity and on the ability of macroscopic shielding currents to establish continuous current loops throughout the structure (Malozemoff, 1989). As shown in the SEM micrographs, the fine-grained morphology and microporosity in the S60 sample hinder the macroscopic circulation of shielding currents, thereby restricting the diamagnetic response predominantly to individual intragranular contributions. By contrast, in the S120 sample, prolonged sintering promotes the growth of platelet-like grains, resulting in enlarged intergranular contact regions and strengthened weak-link coupling, despite the presence of localized macropores in the microstructure. The enhanced intergranular connectivity allows the induced superconducting currents to establish continuous closed-loop over larger effective volumes, thereby substantially improving the overall diamagnetic response and Meissner shielding capability of the S120 sample.

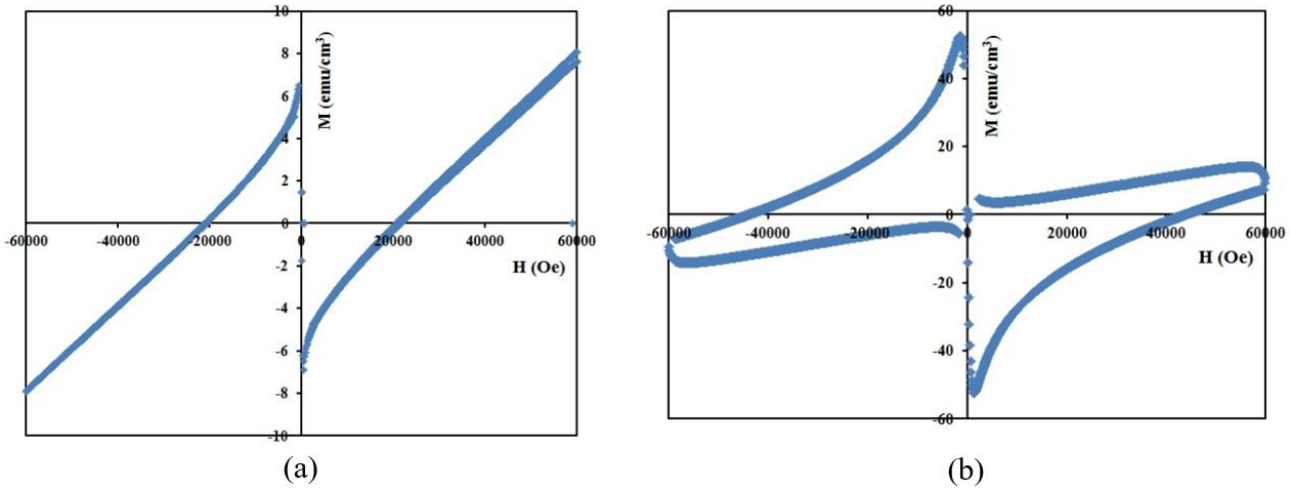

Figure 4. M–H loops measured at (a) 50 K and (b) 10 K for the sample (S60) sintered at 840 ºC for 60 h.

The magnetic-field dependence of magnetization, M(H), for both S60 and S120 samples was measured at 50 K and 10 K in an applied magnetic-field range of ±60,000 Oe (6 T) and the corresponding hysteresis loops are shown in Figures 4 and 5. These measurements provide key information regarding the flux-pinning properties and critical current densities (J_c) of the samples.

M-H loops at 50 K clearly reveal the differences in superconducting behavior between the samples. As shown in the M–H loop of the S60 sample (Figure 4a), the magnetization is small and the high-field response becomes nearly linear with a positive slope, indicating a dominant paramagnetic contribution. At this temperature, thermal fluctuations strongly increases due to the pronounced anisotropy of Bi-2212. The low superconducting volume fraction and weak pinning behavior in the S60 sample lead to a suppressed diamagnetic response, such that the measured signal is largely governed by background contributions arising from non-superconducting paramagnetic impurities and/or unreacted secondary phases.

In the M–H loop of the S120 sample at 50 K (Figure 5a), paramagnetic contribution to magnetization is still dominant. However, the magnetization magnitude is approximately two orders of magnitude higher than that of the S60 sample. This result shows that although the sintering process of 120 h significantly improves intergranular links, thermal fluctuations at 50 K suppress the superconducting fraction.

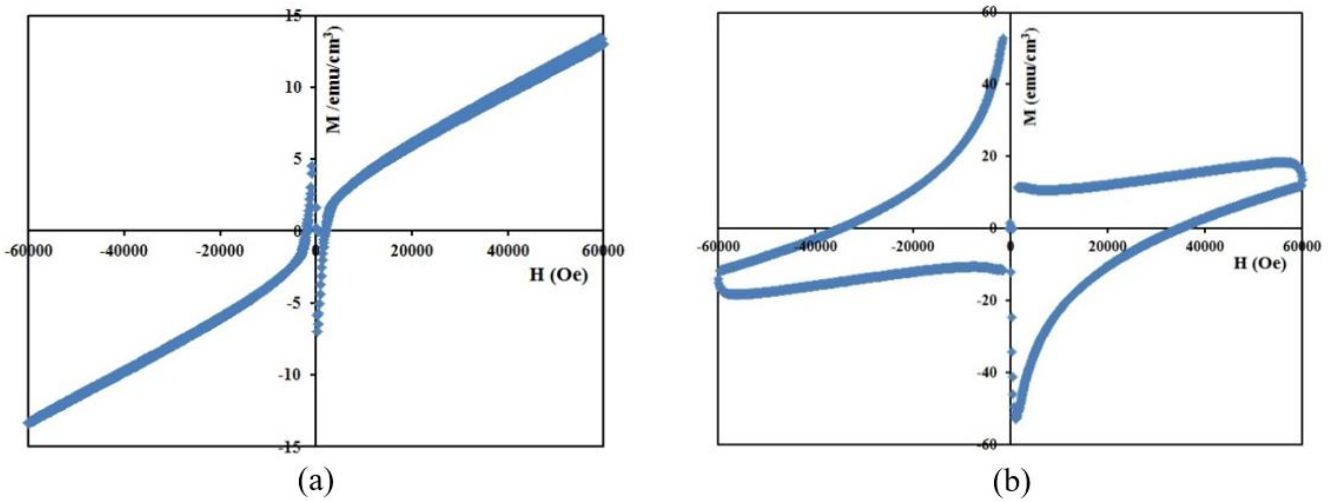

Figure 5. M–H loops measured at (a) 50 K and (b) 10 K for the sample (S120) sintered at 840 °C for 120 h.

At 10 K, thermal activation is strongly suppressed and the superconducting diamagnetic response in both samples completely dominates the paramagnetic background, giving rise to the characteristic symmetric "butterfly-shaped" hysteresis loops which are typical for type-II superconductors (Figures 4b and 5b). The non-closure of the loops up to 60000 Oe (6 T) indicates that the irreversibility field (H_{irr}) at 10 K is well above 6 T for both samples.

The critical current density (J_c) values were calculated according to the Bean formula (Bean, 1964; Gyorgy et al., 1989) and the variation of J_c with the applied magnetic field ($J_c - H$) is shown in Figure 6.

$$J_c = \frac{20\Delta M}{a\left(1-\frac{a}{3b}\right)} \quad (3)$$

where $\Delta M = M^+ - M^-$, a and b are sample dimensions. The a and b dimensions are 3.8 mm and 2.65 mm for S60 sample and 4.1 mm and 2.3 mm for S120 sample, respectively.

According to the Bean critical state model ($J_c \propto \Delta M$), ΔM is directly proportional to both the flux-pinning strength and the critical current-carrying capability. It was found that the ΔM value of the S120 sample near H=0 in the M–H loop at 10 K is larger than that of the S60 sample. The increase in ΔM at 10 K clearly indicates an increase in the critical current density (J_c) in the S120 sample. This trend is in excellent agreement with SEM results, where grain growth and the development of a denser, better-connected microstructure induced by prolonged sintering significantly enhance vortex pinning efficiency.

In polycrystalline HT_c cuprate superconductors, the magnetic-field dependence of J_c can be modeled as the linear superposition of two distinct transport regimes, represented by exponential functions (Peterson & Ekin, 1988): At low magnetic fields, superconducting transport is predominantly governed by the weak-link behavior of intergranular Josephson junctions. At higher fields, however, the phase coherence across these junctions is progressively destroyed, causing the transport mechanism to become dominated by intragranular flux-pinning processes (Hilgenkamp & Mannhart, 2002). To mathematically simulate this complex transport behavior and quantitatively separate individual contributions, the Two-Component Exponential Model is employed (Müller & Matthews, 1993; Peterson & Ekin, 1988). The equation of the model is given by

$$J_c = J_c^{wl}(0)\exp\left(-\frac{H}{H_{wl}}\right) + J_c^{int}(0)\exp\left(-\frac{H}{H_{int}}\right) \quad (4)$$

where $J_c^{wl}(0)$ and $J_c^{int}(0)$ are the zero-field intergranular and intragranular critical current density components, respectively, while H_{wl} and H_{int} denote the characteristic decay fields associated with weak-link coupling and intragranular flux pinning (Ekin et al., 1989; Huang et al., 1998).

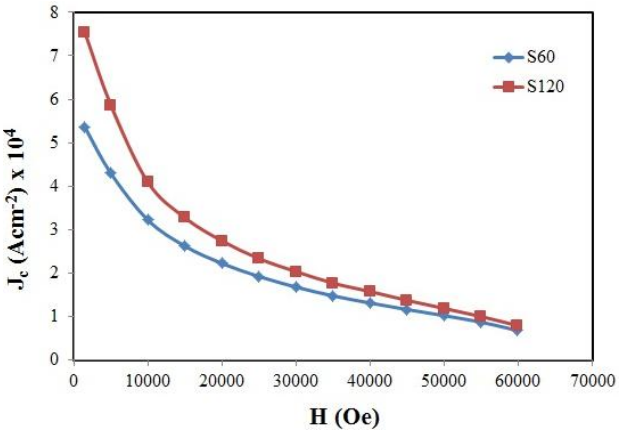

Figure 6. Magnetic-field dependence of the critical current density ($J_c - H$) for Bi-2212 samples sintered at 840 °C for 60 h (S60) and 120 h (S120).

When this semi-empirical model is applied to the experimental $J_c - H$ curves, the resulting parametric data for

the S60 and S120 samples clearly elucidate the microstructural and chemical evolution of the fabricated materials (see Table 1).

Table 1. Semi-empirical fitting parameters obtained from the $J_c - H$ analysis of the S60 and S120 samples at 10 K.

Material	$J_c^{wl}(0)$ (Acm^{-2})	$J_c^{int}(0)$ (Acm^{-2})	H_{wl} (Oe)	H_{int} (Oe)
S60	1.6×10^4	4.1×10^4	1200	38000
S120	2.3×10^4	5.6×10^4	1850	47000

3.1. Low-Field Region (0 < H < 5000 Oe) and Weak-Link Characteristics

As shown in Figure 6, both samples exhibit an extremely sharp and dramatic decrease in J_c with increasing the magnetic field from H = 0. This behavior can be successfully explained within the framework of the first term of the model, namely the J_c^{wl} component, which represents intergranular weak-link transport. In the S60 sample, the grain boundaries formed after a sintering of 60 h are not yet fully optimized in terms of crystallographic coherence and chemical homogeneity. During shorter sintering treatments, the accumulation of secondary phases at grain boundaries suppresses the superconducting order parameter in these regions (Hilgenkamp & Mannhart, 2002). The low H_{wl} value (~1200 Oe) obtained from the model indicates that even relatively small applied magnetic fields rapidly destroy the intergranular Josephson phase coherence, thereby blocking the macroscopic supercurrent flowing through the weak-link network.

Upon prolonging the sintering to 120 h (S120), the total theoretical zero-field critical current $J_c(0)$ increases from ~5.7 × 10^4 Acm^{-2} to 7.9 × 10^4 Acm^{-2}. Notably, both the weak-link term $J_c^{wl}(0)$ and the characteristic field H_{wl} (~1850 Oe) show a pronounced increase. This behavior indicates that the solid-state diffusion occurring during prolonged sintering effectively reduces intergranular voids, suppresses grain-boundary impurity phases and enhances *c*-axis texturing. The consequent reduction in grain misorientation angle strengthens Josephson tunneling across grain boundaries, thereby improving the low-field robustness of the superconducting state (Hilgenkamp & Mannhart, 2002).

3.2. High-Field Region (H > 10000 Oe) and Flux-Pinning Mechanism

In contrast to the sharp degradation observed at low magnetic fields, J_c exhibits a gradual and slower suppression rate in the high magnetic field region (H > 1000 Oe). In high-field region, the intergranular weak-link network becomes effectively dephased, $\exp(-H/H_{wl}) \to 0$ and superconducting current transport is dominated entirely by the second term of the model, the intragranular current-carrying component (J_c^{int}) (Ekin et al., 1989). The slower decreasing trend implies a strong resistance of effective vortex-pinning centers in the microstructure against applied magnetic fields. The superior J_c performance of the S120 sample in the high-field region indicates an enhanced flux pinning capability. According to the semi-empirical model, the higher H_{int} value obtained for the S120 sample (47000 Oe) compared to the S60 sample (38000 Oe) provides strong evidence that prolonged sintering not only enhances grain-boundary quality but also substantially improves the intragranular crystal matrix.

The results derived from the semi-empirical modeling are closely linked to the solid-state reaction kinetics and vortices in Bi-2212 superconductors. Due to the extremely large anisotropy of the Bi-2212 phase (γ>50), magnetic flux lines do not form continuous 3D-vortex structures in the material; instead, they become confined as quasi-2D "pancake vortices" localized in the CuO_2 planes (Blatter et al., 1994). At low temperatures such as 10 K, thermal fluctuations are insufficient to mobilize these pancake vortices, causing them to remain trapped at point-like defects in the superconducting matrix. If these vortices are not effectively pinned, the Lorentz force generated by the macroscopic transport current drives vortex motion (flux flow), resulting in dissipative energy losses and the local destruction of the superconducting state (Blatter et al., 1994; Fisher et al., 1991).

The higher $J_c^{int}(0)$ and H_{int} values obtained for the S120 sample indicate that prolonged sintering leads to an optimized and spatially homogeneous distribution of cationic disorder and oxygen vacancies (δ) in the crystal lattice. Point-like lattice defects and microscopic dislocations with characteristic dimensions comparable to the extremely short coherence length of Bi-2212 (ξ_{ab} ~2 nm) act as strong potential wells (pinning centers) for pancake vortices. The stable and slowly decreasing behavior observed in the high-field region of Figure 6 suggests that the vortex system is not in a weakly pinned and ordered Bragg glass phase, but rather becomes in a strongly disordered vortex glass phase capable of maintaining superconducting integrity under high magnetic fields (Fisher et al., 1991). The high intragranular flux-pinning field (H_{int}) extracted from the semi-empirical model shows that the point-like defects optimized with a sintering of 120 h reinforce the Josephson coupling between 2D pancake vortices, thereby stabilizing coherent 3D vortex-line formations. This strong collective pinning substantially enhances the resistance of the vortex system against the Lorentz force under high magnetic fields,

while significantly suppressing thermally and current-activated vortex creep. As a result, the locking of the system into the vortex glass phase directly guarantees superior current-carrying stability under the high magnetic fields.

3.3. Vortex Glass Phase and the Role of Point Defects

Semi-empirical analysis of the $J_c - H$ characteristics of the S60 and S120 samples at 10 K indicates that prolonged sintering improves superconducting performance through a dual mechanism:

Macroscopic Level: Chemical purification of grain boundaries and improved structural texturing enhance the Josephson weak-link current-carrying capacity (J_c^{wl}), leading to an increase in zero-field critical current density and an improvement in stability in the low-field region (Hilgenkamp & Mannhart, 2002).

Microscopic Level: The optimization of intragranular defect structures and oxygen stoichiometry enhances the stability of pinning centers (H_{int}). In the high-field region, it strengthens the resistance of 2D pancake vortices against the Lorentz force, resulting in a significantly reduced critical current decreasing rate (Blatter et al., 1994; Fisher et al., 1991).

These results provide semi-empirical and theoretical evidence that prolonged sintering is a critical processing parameter for Bi-2212 bulk superconductors in practical high-field magnet applications, as it simultaneously enhances intergranular weak-link connectivity and stabilizes intragranular vortex dynamics.

4. Conclusion

In this study, the effects of sintering time (60 h and 120 h) on the structural, microstructural and magneto-transport properties of bulk $Bi_2Sr_2CaCu_2O_{8+\delta}$ (Bi-2212) HT_c superconductors were investigated by experimental characterization and a semi-empirical Two-Component Exponential Model in detail. The results clearly show that the sintering of 120 h at 840 °C optimizes the superconducting properties of the material through a dual-scale improvement, affecting both macroscopic and microscopic levels. Structural analyses revealed that prolonging the sintering duration from 60 h to 120 h largely eliminates performance-limiting secondary impurity phases, such as $BiSr_3O_{5.4}$ and $Bi_2Ca_2O_5$, thereby improving phase purity. The thermally activated and controlled oxygen desorption occurring during the heat treatment expands the *c*-axis, shifting the system from the overdoped regime to the optimally doped regime associated with enhanced superconducting performance. This optimization balances the carrier concentration in the CuO_2 planes, thereby establishing a microscopic origin for the enhancement of the critical current density. Furthermore, the increase in crystallite size accompanied by the decrease in microstrain indicates the reduction of lattice defects and the improvement of crystalline quality. SEM micrographs confirmed that prolonged sintering develops the anisotropic platelet-like grain morphology characteristic of the Bi-2212 system, while simultaneously promoting stronger mechanical interlocking between adjacent grains. Two-component exponential modelling analysis of the transport mechanism further revealed that the 120 h sintering treatment improves low-field stability and enhances the Josephson weak-link current-carrying capacity (J_c^{wl}) through effective grain-boundary purification at the macroscopic level. At the microscopic scale, the optimization of intragranular nanoscale defects and oxygen vacancies increases the stability of flux-pinning centers (H_{int}), thereby providing strong resistance against the field-induced motion of 2D pancake vortices under high magnetic fields. In conclusion, the optimization of the solid-state reaction duration has been identified as a critical processing parameter for enhancing the application potential of Bi-2212-based bulk superconductors in large-scale engineering applications, including practical high-field magnet technologies, superconducting wires and tape industries.

Conflict of Interest

The authors declare that they have no conflict of interest.

Disclosure of Generative AI Use

An AI tool was used partially during the translation process.

References

Argyriou, D. N., Garcia, J. A., Mitchell, J. F., Jorgensen, J. D., & Hinks, D. G. (1996). Phase development of Bi-2212 superconductor: A time-resolved neutron powder diffraction investigation. *Journal of Materials Research*, *11*(2), 277-280. https://doi.org/10.1557/JMR.1996.0032

Bean, C. P. (1964). Magnetization of high-field superconductors. *Reviews of Modern Physics*, *36*(1), 31. https://doi.org/10.1103/RevModPhys.36.31

Blatter, G., Feigel'man, M. V., Geshkenbein, V. B., Larkin, A. I., & Vinokur, V. M. (1994). Vortices in high-temperature superconductors. *Reviews of Modern Physics*, *66*(4), 1125. https://doi.org/10.1103/RevModPhys.66.1125

Clem, J. R. (1991). Two-dimensional vortices in a stack of thin superconducting films: A model for high-temperature superconducting multilayers. *Physical Review B*, *43*(10), 7837. https://doi.org/10.1103/PhysRevB.43.7837

Ekin, J. W., Larson, T. M., Hermann, A. M., Sheng, Z. Z., Togano, K., & Kumakura, H. (1989). Double-step behavior of critical current vs. magnetic field in Y-, Bi- and Tl-based bulk high-T_c superconductors. *Physica C:*

Superconductivity, *160*(5-6), 489-496. https://doi.org/10.1016/0921-4534(89)90425-5

Fisher, D. S., Fisher, M. P., & Huse, D. A. (1991). Thermal fluctuations, quenched disorder, phase transitions, and transport in type-II superconductors. *Physical Review B*, *43*(1), 130. https://doi.org/10.1103/PhysRevB.43.130

Garnier, V., Caillard, R., Sotelo, A., & Desgardin, G. (1999). Relationship among synthesis, microstructure and properties in sinter-forged Bi-2212 ceramics. *Physica C: Superconductivity*, *319*(3-4), 197-208. https://doi.org/10.1016/S0921-4534(99)00308-1

Gyorgy, E. M., Van Dover, R. B., Jackson, K. A., Schneemeyer, L. F., & Waszczak, J. V. (1989). Anisotropic critical currents in Ba2YCu3O7 analyzed using an extended Bean model. *Applied Physics Letters*, *55*(3), 283-285. https://doi.org/10.1063/1.102387

Heeb, B., Gauckler, L. J., Heinrich, H., & Kostorz, G. (1993). From imperfect to perfect $Bi_2Sr_2CaCu_2O_x$ (Bi–2212) grains. *Journal of Materials Research*, *8*(9), 2170-2176. https://doi.org/10.1557/JMR.1993.2170

Hilgenkamp, H., & Mannhart, J. (2002). Grain boundaries in high-T_c superconductors. *Reviews of Modern Physics*, *74*(2), 485. https://doi.org/10.1103/RevModPhys.74.485

Huang, Y. K., ten Haken, B., & ten Kate, H. H. (1998). Critical current of high T_c superconducting Bi2223/Ag tapes. *Physica C: Superconductivity*, *309*(3-4), 197-202. https://doi.org/10.1016/S0921-4534(98)00608-X

Kametani, F., Shen, T., Jiang, J., Scheuerlein, C., Malagoli, A., Di Michiel, M., Huang, Y., Miao, H., Parrell, J. A., Hellstrom, E. E., & Larbalestier, D. C. (2011). Bubble formation within filaments of melt-processed Bi2212 wires and its strongly negative effect on the critical current density. *Superconductor Science and Technology*, *24*(7), 075009. https://doi.org/10.1088/0953-2048/24/7/075009

Liang, J. K., Xie, S. S., Che, G. C., Huang, J. Q., Zhang, Y. L., & Zhao, Z. X. (1988). Crystal structure and superconductivity of $Bi_2Sr_2CaCu_2O_8$ compound. *Modern Physics Letters B*, *2*(01), 483-489. https://doi.org/10.1142/S0217984988000059

Maeda, H., Tanaka, Y., Fukutomi, M., & Asano, T. (1988). A new high-T_c oxide superconductor without a rare earth element. *Japanese Journal of Applied Physics*, *27*(2A), L209. https://doi.org/10.1143/JJAP.27.L209

Malozemoff, A. P. (1989). Macroscopic magnetic properties of high temperature superconductors. In D. M. Ginsberg (Ed.), *Physical properties of high temperature superconductors I* (pp. 71-150). World Scientific. https://doi.org/10.1142/0675

Müller, K. H., & Matthews, D. N. (1993). A model for the hysteretic critical current density in polycrystalline high-temperature superconductors. *Physica C: Superconductivity*, *206*(3-4), 275-284. https://doi.org/10.1016/0921-4534(93)90526-V

Özçelik, B., Özkurt, B., Yakıncı, M. E., Sotelo, A., & Madre, M. A. (2013). Relationship between annealing time and magnetic properties in Bi-2212 textured composites. *Journal of Superconductivity and Novel Magnetism*, *26*(4), 873-878. https://doi.org/10.1007/s10948-012-1874-9

Peterson, R. L., & Ekin, J. W. (1988). Josephson-junction model of critical current in granular $Y_1Ba_2Cu_3O_{7-\delta}$ superconductors. *Physical Review B*, *37*(16), 9848. https://doi.org/10.1103/PhysRevB.37.9848

Ross, D. K. (2005). A determination of the variation in the lattice parameters of $Bi_2Sr_2CaCu_2O_{8+x}$ (Bi-2212) as a function of temperature and oxygen content. *Physica C: Superconductivity*, *425*(3-4), 130-134. https://doi.org/10.1016/j.physc.2005.06.016

Scherrer, P. (1918). Estimation of the size and internal structure of colloidal particles by means of röntgen. *Nachrichten von der Gesellschaft der Wissenschaften zu Göttingen*, *2*, 96-100.

Tarascon, J. M., McKinnon, W. R., Barboux, P., Hwang, D. M., Bagley, B. G., Greene, L. H., Hull, G. W., LePage, Y., Stoffel, N., & Giroud, M. (1988). Preparation, structure, and properties of the superconducting compound series $Bi_2Sr_2Ca_{n-1}Cu_nO_y$ with n=1,2, and 3. *Physical Review B*, *38*(13), 8885. https://doi.org/10.1103/PhysRevB.38.8885

Wang, G., Raine, M. J., & Hampshire, D. P. (2018). The cause of 'weak-link'grain boundary behaviour in polycrystalline $Bi_2Sr_2CaCu_2O_8$ and $Bi_2Sr_2Ca_2Cu_3O_{10}$ superconductors. *Superconductor Science and Technology*, *31*(2), 024001. https://doi.org/10.1088/1361-6668/aaa1b8

Yang, H., Shahzad, M. B., Yu, X., & Qi, Y. (2016). Influence mechanism of secondary gel technique on Bi-2212 superconducting phase: Gel model simulation and verification. *Materials & Design*, *99*, 115-119. https://doi.org/10.1016/j.matdes.2016.03.051

Zhang, Y., Yang, H., Li, M., Sun, B., & Qi, Y. (2010). Improvement of multiple oxide properties: Effect of gel processes on the quality of $Bi_2Sr_2CaCu_2O_{8+\delta}$ superconducting powders. *CrystEngComm*, *12*(10), 3046-3051. https://doi.org/10.1039/B927276C